OPEN ACCESS
[DOI]10.12016/j.issn.2096-1456.202660187

·生物材料专栏 基础研究·

负载芍药苷的PCL/COL静电纺丝膜对MC3T3-E1成骨性能的影响

李泽卉[1]，　刘朝辉[2]，　杨毓哲[1]，　张宾[1]，　张云涛[1]
1.山东医药大学附属医院口腔修复科，山东 滨州（256600）；　2.广饶县人民医院口腔科，山东 东营（257000）

【摘要】　目的　探讨负载芍药苷（PF）的聚己内酯/胶原蛋白（PCL/ COL）静电纺丝膜的适宜载药浓度，评价其理化性能、生物相容性及促成骨效应，为骨组织工程支架的研发提供实验依据。**方法**　采用静电纺丝技术制备PCL膜（PCL组）、PCL/COL膜（PCL/COL组），以及负载低、中、高药物浓度芍药苷（0.1、0.2、0.4 mg/mL）的PCL/COL膜（PCL/COL-PF_L组、PCL/COL-PF_M组及PCL/COL-PF_H组）。通过扫描电镜（SEM）、傅里叶变换红外光谱（FTIR）、静态接触角测量、体外药物释放及体外降解实验评估各组静电纺丝膜的材料学性能。将MC3T3-E1细胞分别与各组静电纺丝膜共培养，通过CCK-8法、活/死细胞染色及罗丹明-鬼笔环肽染色分别检测各组静电纺丝膜对MC3T3-E1细胞增殖、细胞毒性及细胞骨架形态的影响；采用碱性磷酸酶（ALP）染色及活性检测、茜素红染色（ARS）评估各组静电纺丝膜对MC3T3-E1细胞早期成骨分化与矿化程度的影响；采用RT-qPCR和Western blot检测各组静电纺丝膜对MC3T3-E1细胞的成骨相关转录因子2（Runx2）和骨保护素（OPG）的mRNA及蛋白表达的影响。**结果**　扫描电镜下各组静电纺丝膜纤维分布均匀，纤维直径主要分布在300~800 nm。FTIR结果显示，PCL、COL及芍药苷的特征吸收峰均可被检测到，表明芍药苷已成功负载于PCL/COL静电纺丝膜中，且各组分化学结构未发生明显改变。静态接触角表明，与PCL组相比，PCL/COL、PCL/COL-PF_L、PCL/COL-PF_M与PCL/COL-PF_H组接触角显著减小（P<0.001），亲水性显著提高。体外药物释放实验显示，PCL/COL-PF_L组、PCL/COL-PF_M组及PCL/COL-PF_H组静电纺丝膜在第1天表现出明显的突释现象，随后释药速率逐渐降低，并于第7天后趋于稳定。体外降解实验表明，PCL膜降解缓慢，第12周剩余质量比82.67%±0.38%，引入COL后降解速率较PCL组明显加快，PCL/COL组剩余质量比降至56.63%±0.68%（P<0.001），进一步引入芍药苷（PF）后较PCL组降解速率提升，PCL/COL-PF_L、PCL/COL-PF_M及PCL/COL-PF_H组第12周剩余质量比分别降至50.94%±0.74%、50.84%±1.39%和50.33%±0.75%（P<0.01）。CCK-8结果显示，PCL/COL、PCL/COL-PF_L及PCL/COL-PF_M组相较PCL组均能促进细胞增殖（P<0.001）；而PCL/COL-PF_H组第7天显著抑制细胞增殖（P<0.001）。活/死细胞染色与罗丹明-鬼笔环肽染色结果显示各组静电纺丝膜均具有良好的生物相容性且形态清晰。成骨实验结果表明，与PCL组相比，PCL/COL-PF_L组及PCL/COL-PF_M组ALP活性显著升高（P<0.001），矿化结节沉积增多。Runx2、OPG的mRNA及蛋白表达显著上调（P<0.01），其中PCL/COL-PF_M组效果最显著（P<0.001）。**结论**　静电纺丝法制备的负载芍药苷的PCL/COL静电纺丝膜具有良好的理化和生物相容性，其中0.2 mg/mL载药组（PCL/COL-PF_M）促成骨效果最佳，为芍药苷在骨组织工程的局部递送应用提供了实验依据。

【关键词】　芍药苷；　聚己内酯；　胶原蛋白；　静电纺丝；　骨组织工程；　药物缓释；　MC3T3-E1细胞；　成骨
【中图分类号】　R78　**【文献标志码】**　A　**【文章编号】**　2096-1456（2026）11-1075-13
【引用著录格式】　李泽卉，刘朝辉，杨毓哲，等. 负载芍药苷的PCL/COL静电纺丝膜对MC3T3-E1成骨性能的影响[J]. 口腔疾病防治, 2026, 34(11): 1075-1087. doi:10.12016/j.issn.2096-1456.202660187.

微信公众号

【收稿日期】2026-05-20；　**【修回日期】**2026-09-03
【基金项目】山东省自然科学基金（ZR2023MH039）；滨州医学院附属医院科研计划项目（BY2021KJ10）；国家级大学生创业课题（202310440160）
【作者简介】李泽卉，硕士，Email：908052036@qq.com
【通信作者】张云涛，副教授，硕士，Email：Zytao999@163.com；张宾，副主任医师，硕士，Email：410055090@qq.com

Effect of paeoniflorin-loaded PCL/COL electrospun membranes on osteogenic activity in MC3T3-E1 cells

LI Zehui[1], LIU Zhaohui[2], YANG Yuzhe[1], ZHANG Bin[1], ZHANG Yuntao[1]. 1. Department of Prosthodontics, Affiliated Hospital of Shandong Medical University, Binzhou 256600, China; 2. Department of Stomatology, Guangrao County People's Hospital, Dongying 257000, China
Corresponding author: ZHANG Yuntao, Email: Zytao999@163.com; ZHANG Bin, Email:410055090@qq.com

【Abstract】 Objective To investigate the appropriate loading concentration of paeoniflorin in polycaprolactone/collagen (PCL/COL) nanofiber sustained-release scaffolds; to evaluate their physicochemical properties, biocompatibility, and osteogenic effects; and to provide an experimental basis for the development of scaffolds for bone tissue engineering. **Methods** Electrospun PCL membranes (PCL group), PCL/COL composite membranes (PCL/COL group), and PCL/COL membranes loaded with paeoniflorin at low, medium, and high concentrations (0.1, 0.2, and 0.4 mg/mL, designated as the PCL/COL-PF_L, PCL/COL-PF_M, and PCL/COL-PF_H groups, respectively) were fabricated by electrospinning. The material properties of the electrospun membranes were evaluated by scanning electron microscopy (SEM), Fourier transform infrared spectroscopy (FTIR), static water contact angle measurement, *in vitro* drug release assays, and *in vitro* degradation testing. MC3T3-E1 cells were separately co-cultured with various electrospun membranes, and the effects of the electrospun membranes on MC3T3-E1 cell proliferation, cytotoxicity, and cytoskeletal morphology were assessed by CCK-8 assays, live/dead cell staining, and rhodamine-phalloidin staining, respectively. Early osteogenic differentiation and mineralization of MC3T3-E1 cells were examined by alkaline phosphatase (ALP) staining and activity assays, and Alizarin Red S (ARS) staining. The mRNA expression of Runt-related transcription factor 2 (Runx2) and osteoprotegerin (OPG) in MC3T3-E1 cells treated with electrospun membranes in each group was detected by reverse transcription quantitative real-time PCR (RT-qPCR), and the protein expression levels of the osteogenesis-related proteins Runx2 and OPG were determined by Western blotting. **Results** SEM revealed that the fibers of the electrospun membranes in all the groups were uniformly distributed, with fiber diameters predominantly in the range of 300-800 nm. FTIR results showed that the characteristic absorption peaks of PCL, COL, and paeoniflorin could all be detected, indicating that paeoniflorin had been successfully loaded into the PCL/COL electrospun membranes and that the chemical structure of each component had not been significantly altered. Static contact angle measurements revealed that, compared with the PCL group, the contact angles of the PCL/COL, PCL/COL-PF_L, PCL/COL-PF_M, and PCL/COL-PF_H groups were significantly decreased ($P < 0.001$), demonstrating markedly improved hydrophilicity. In vitro drug release experiments showed that the PCL/COL-PF_L, PCL/COL-PF_M, and PCL/COL-PF_H groups exhibited a pronounced burst release on day 1, followed by a gradual decrease in the release rate, which stabilized after day 7. The *in vitro* degradation study showed that the PCL membranes degraded slowly, with a residual mass ratio of 82.67% ± 0.38% at week 12. After the incorporation of COL, the degradation rate was significantly accelerated compared with the PCL group, with the residual mass ratio of the PCL/COL group decreasing to 56.63% ± 0.68% ($P < 0.001$). After paeoniflorin incorporation, the degradation rate was further increased relative to the PCL group, with the residual mass ratios of the PCL/COL-PF_L, PCL/COL-PF_M, and PCL/COL-PF_H groups decreasing at week 12 to 50.94% ± 0.74%, 50.84% ± 1.39%, and 50.33% ± 0.75%, respectively ($P < 0.01$). CCK-8 results showed that, compared with the PCL group, the PCL/COL, PCL/COL-PF_L, and PCL/COL-PF_M groups significantly promoted cell proliferation ($P < 0.001$). The proliferative activity of the PCL/COL-PF_H group showed significant inhibitory effect on day 7 ($P < 0.001$). The results of the live/dead cell staining and rhodamine-phalloidin staining indicated that the electrospun membranes in all the groups exhibited good biocompatibility and well-defined cell morphology. Osteogenic experiments demonstrated that, compared with the PCL group, the PCL/COL-PF_L and PCL/COL-PF_M groups showed significantly increased ALP activity ($P < 0.001$), enhanced deposition of mineralized nodules, and significantly upregulated mRNA and protein expression of Runx2 and OPG ($P < 0.01$), with the most pronounced effects observed in the PCL/COL-PF_M group ($P < 0.001$). **Conclusions** The paeoniflorin-loaded PCL/COL electrospun membranes exhibited favorable physicochemical properties and good biocompatibility. Among them, the 0.2 mg/mL loading group (PCL/COL-PF_M) showed the most pronounced pro-osteogenic effect, providing an experimental basis for the local delivery of paeoniflorin in bone tissue engineering applications.

【Key words】 paeoniflorin; polycaprolactone; collagen; electrospinning; bone tissue engineering; sustained drug release; MC3T3-E1 cells; osteogenesis
J Prev Treat Stomatol Dis, 2026, 34(11): 1075-1087.

骨损伤是口腔颌面外科及骨科临床常见问题，严重创伤、感染及肿瘤切除等均可导致大面积骨组织缺损，影响患者的咀嚼功能及生活质量[1-2]。目前临床上自体骨移植和异体骨移植均存在供体来源有限、免疫排斥反应和疾病传播的风险[3]。因此，开发兼具稳定成骨性能与良好生物相容性的人工骨替代材料，已成为骨组织工程领域的重要研究方向。

静电纺丝技术是一种先进的纳米纤维材料制备方法。该技术所制备的支架微表面结构尺寸较小（比表面积可达到 100 m^2/g 以上），孔隙大且相互连通（孔隙率＞80%）[4-5]，能够高度还原和模拟天然骨的细胞外基质（extracellular matrix，ECM）的拓扑结构及生物化学特性，可以提供良好的细胞黏附位点（黏附率增加 40%～60%），提高成骨细胞增殖（增殖率增加 30%～50%）和定向分化（碱性磷酸酶活性提高 2～3 倍）[6-7]。聚己内酯（polycaprolactone，PCL）具有良好的可降解性能[8]。但PCL疏水性强、降解速度慢等缺点限制了其在组织工程中的应用[9]。胶原蛋白（collagen，COL）具有优异的低免疫原性、生物相容性与可降解性[10]，可以有效改善PCL支架的生物学性能[11]。因此，本研究选择PCL/COL复合材料作为静电纺丝膜的基体材料，以期构建兼具良好力学性能的骨组织工程支架。

芍药苷（Paeoniflorin，PF）是一种来源于芍药科中药的单萜苷类化合物，具有低毒性和良好的安全性。研究表明，芍药苷剂量依赖性地上调Runt相关转录因子2（Runt-related transcription factor 2，Runx2），Runx2的表达促进成骨细胞分化[12]。但其体内代谢较快，局部有效药物浓度维持时间较短，限制了其临床应用。尽管已有多种天然活性单体被负载于静电纺丝膜用于骨组织工程研究[13]，但关于芍药苷负载PCL/COL静电纺丝膜的研究仍较少，其药物缓释行为及促成骨作用尚缺乏系统评价。

综上，本实验构建负载芍药苷的PCL/COL静电纺丝膜，旨在制备具有药物缓释作用且生物学性能优良的复合支架，提高药物利用率。通过体外细胞实验评价其生物相容性与成骨活性，以期为芍药苷在骨组织工程中的局部递送应用提供实验依据。

1　材料和方法

1.1　主要材料和仪器

芍药苷（MB1948-20MG，美仑生物，中国）；胶原蛋白（MB5213-2，美仑生物，中国）；聚己内酯（MB2453，安诺伦生物，中国）；小鼠颅骨成骨细胞（mouse calvaria osteoblastic cell line，MC3T3-E1）（20220330A1，美仑生物，中国）；α-MEM培养（MA0216，美仑生物，中国）；牛血清白蛋白BSA（A8010，索莱宝，中国）；胎牛血清（PWL001，美仑，中国）；CCK-8试剂盒（C0048FT，美仑生物，中国）；MC3T3-E1成骨诱导培养基（MUXMT-90021，赛业，中国）；碱性磷酸酶活性检测试剂盒（P0321S，碧云天，中国）；Western及IP细胞裂解液（P0013J，碧云天，中国）；碱性磷酸酶显色试剂盒（C3206，碧云天，中国）；Calcein-AM/PI染色/碘化丙啶（propidium iodide，PI）细胞活性与细胞毒性检测试剂盒（C2015S，碧云天，中国）；茜素红染色液（0.2%，pH=8.3）（2311003，索莱宝，中国）；罗丹明标记鬼笔环肽（CA1610-300T，索莱宝，中国）；4′，6-二脒基-2-苯基吲哚（4′，6-diamidino-2-phenylindole，DAPI）（C1002，碧云天，中国）；TRIzol试剂（15596018，Invitrogen，美国）；逆转录试剂盒（D7168S，碧云天，中国）；SYBR® Green（D7260，碧云天，中国）；兔抗小鼠Runx2单克隆抗体（12556S，稀释比例1∶1 000，CST，美国）；兔抗小鼠骨保护素（osteoprotegerin，OPG）多克隆抗体（GTX127948，稀释比例1∶1 000，GeneTex，美国）；小鼠抗甘油醛-3-磷酸脱氢酶（glyceraldehyde-3-phosphate dehydrogenase，GAPDH）单克隆抗体（AF0006，稀释比例1∶1 000，碧云天，中国）；辣根过氧化物酶（horseradish peroxidase，HRP）标记的山羊抗兔IgG二抗（P0948，稀释比例1∶2 000，碧云天，中国）；HRP标记的山羊抗小鼠IgG二抗（A0216，稀释比例1∶2 000，碧云天，中国）。

高压电源（TE4020，泰思曼，中国）；微量注射泵（WGS-1020，威高，中国）；扫描电镜（Sigma 300-VP，蔡司，德国）；真空干燥箱（DZF-6050，一恒，中国）；酶标仪（MULTISKAN FC，Thermo，美国）；接触角测量仪（OCA25，奥德利诺，德国）；超微量紫外可见分光光度计（K5600C，凯奥，中国）；傅里叶变换红外光谱仪（IRPrestige-21，岛津，日本）；激光共聚焦显微镜（TCS-SPE，Leica，德国）；PCR仪（CFX96 Touch Bio-rad，美国）；TC处理（tissue cul-

ture treated）6孔细胞培养板（803006-18，赛普，中国）；TC处理12孔细胞培养板（803012-18，赛普，中国）；TC处理24孔细胞培养板（803024-18，赛普，中国）。

1.2　负载芍药苷的静电纺丝的制备及其理化性能检测

1.2.1　制备静电纺丝膜　称取0.75 g PCL溶于5 mL六氟异丙醇中，制备浓度为150 mg/mL PCL组的静电纺丝液；将COL与PCL按质量比1∶3的比例溶于5 mL六氟异丙醇中，制备浓度为150 mg/mL PCL/COL组的静电纺丝液；配制PCL/COL组静电纺丝液15 mL，分为3份，每份5 mL，分别加入0.5、1、2 mg芍药苷，得到浓度分别为0.1、0.2、0.4 mg/mL的3组静电纺丝液，用于制备PCL/COL-PF_L组、PCL/COL-PF_M组、PCL/COL-PF_H组。

吸取上述各组5 mL溶液，安装至微量注射泵，连接内径0.5 mm的针头，调节针头与带锡箔纸的接收滚筒的距离为20 cm、高压电源的电压为18 kV，推进速度为1 mL/h。设置环境温度在25 ℃，湿度在50%以下制备静电纺丝，每组制备5张。完成制备后取下锡箔纸，于干燥箱40 ℃中放置24 h。将制备的静电纺丝膜裁剪为适于孔板孔径的尺寸，用于后续实验。

1.2.2　扫描电镜观察各组静电纺丝膜的微观形貌　各组取1张2.0 cm×2.0 cm的静电纺丝膜，用导电胶将各组纤维膜固定于扫描电镜（scanning electron microscope，SEM）的载物台上，支架表面镀金处理，SEM下观察纤维形貌。每组随机选取3个视野，每张视野中随机选40根纤维，利用Nano Measurer软件分析各组纳米纤维直径。

1.2.3　静电纺丝膜的傅里叶变换红外光谱检测　对静电纺丝膜及芍药苷原料粉末进行化学结构表征。分别取芍药苷粉末及载0.1、0.2、0.4 mg/mL PF浓度的PCL/COL静电纺丝膜各5 mg，与溴化钾压片后置于载物架上，以溴化钾为背景，扫描4 000~400 cm^{-1}，得到红外光谱。

1.2.4　静电纺丝膜的静态接触角检测　各组取1张3.0 cm×3.0 cm的静电纺丝膜，平整贴于载玻片上，置于样品台。通过微量注射器在膜表面滴加超纯水16 μL，待液滴稳定后，分别于滴加后2 s（初始接触角）和5 min（平衡接触角）拍摄液滴形貌图像，采用仪器配套软件测量接触角。每组测量3个不同位置，取平均值。接触角越小，表明材料亲水性越好。

1.2.5　静电纺丝膜的体外药物释放情况　配制芍药苷标准溶液（0.5、1、5、10、20 μg/mL），测定230 nm处的吸光度以绘制芍药苷曲线。PCL/COL-PF_L组、PCL/COL-PF_M组、PCL/COL-PF_H组各取1张15 mg静电纺丝膜，置于PBS溶液中，于100 r/min，37 ℃条件下振荡培养。于第1、3、5、7、11、15、21天吸取5 mL释放液，测定230 nm处吸光度，并再次加入5 mL新鲜PBS溶液。V为释放介质体积（5 mL），C_1为各时间节点标准曲线所求得的药物浓度（μg/mL），W为芍药苷的理论总质量。药物的累积释放量等于每一个时间节点的药物释放率R的代数和，将获得的数据绘制药物累积释放曲线。计算药物释放率：$R=(V\times C_1)/W\times 100\%$[14]。

1.2.6　静电纺丝膜的体外降解情况　将各组静电纺丝膜裁剪成10 mm×10 mm大小，测定PCL、PCL/COL、PCL/COL-PF_L、PCL/COL-PF_M、PCL/COL-PF_H膜的初始重量W_0。样品浸泡于含100 μg/mL Ⅰ型胶原酶的PBS溶液中，置于37 ℃恒温培养箱中，共观察12周。每隔2周取出同一样品，烘干后测定质量W_1，质量变化根据以下公式计算：剩余质量比（%）$=W_1/W_0\times 100\%$[15]。

1.3　评价静电纺丝纤维膜的体外生物相容性及成骨分化潜能

1.3.1　CCK-8检测　MC3T3-E1细胞培养于含10%胎牛血清和1%青霉素-链霉素双抗的α-MEM完全培养基中，置于37 ℃、5%CO_2培养箱内培养。将各组静电纺丝膜裁剪成20 mm直径圆片，铺于6个24孔板内，每组设置5个复孔。膜片用75%乙醇浸泡60 s，正反面紫外线光照各2 h。用直径为12 mm高压灭菌后的不锈钢环将静电纺丝膜压于孔底，用PBS清洗3次，吸出PBS，赶走底部气泡，使薄膜紧贴板底，取出不锈钢环。MC3T3-E1细胞以2×10^4个/孔接种于薄膜上，待24 h细胞贴壁后，于避光环境下每孔更换100 μL含10%CCK-8溶液的培养基。避光孵育1 h，用酶标仪在450 nm处检测吸光度（OD值）。第1、4、7天同一时间重复上述操作。

根据CCK-8检测结果，选取生物相容性较好的PCL、PCL/COL、PCL/COL-PF_L、PCL/COL-PF_M四组静电纺丝用于后续成骨分化相关实验。

1.3.2　活/死细胞染色　MC3T3-E1细胞培养方法及各组静电纺丝膜的裁剪、灭菌及固定方法同1.3.1。将各组静电纺丝膜片铺于1个24孔板内，每组设置3个复孔。MC3T3-E1细胞以2×10^4个/孔接种于薄膜上。细胞贴壁24 h后，根据碧云天活/死细胞

染色试剂盒配制工作液，每孔加入700 μL工作液，避光孵育30 min后，于荧光倒置显微镜下观察并拍照。

1.3.3　罗丹明-鬼笔环肽染色　MC3T3-E1细胞培养及各组膜的裁剪、灭菌及固定方法同1.3.1。将各组膜片铺于1个24孔板内，每组设置3个复孔。待细胞贴壁24 h后，弃去培养基，PBS清洗3次，经4%多聚甲醛溶液固定10 min，PBS冲洗3次，使用0.5%的TritonX-100溶液进行细胞膜透膜处理5 min，PBS冲洗3次。每孔加入500 μL的含1%牛血清白蛋白的罗丹明标记鬼笔环肽染液（5 μg/mL），避光孵育30 min。随后用DAPI溶液（100 nmol/L）对细胞核进行复染1 min，PBS清洗。于荧光倒置显微镜下观察并拍照。

1.3.4　碱性磷酸酶染色与活性测定　实验分为染色观察与活性定量两部分，前者使用12孔板，后者使用24孔板。MC3T3-E1细胞培养方法与各组静电纺丝膜的裁剪、灭菌及固定方法同1.3.1。碱性磷酸酶（alkaline phosphatase，ALP）染色：将各组静电纺丝膜裁剪、灭菌后铺于1个12孔板内，每组设置3个复孔。MC3T3-E1细胞以3×10^{4}个/孔的密度接种于膜表面，待细胞贴壁24 h后，按说明书更换为上述成骨诱导培养基，每2 d换液1次。培养7 d后，移除培养基，PBS清洗2次，按照ALP染色试剂盒说明书配制染色工作液，每孔加入适量染色液，室温避光孵育15～30 min，弃去染色液，PBS清洗2次，于倒置显微镜下观察并拍照。ALP活性定量：将各组静电纺丝膜裁剪、灭菌后铺于1个24孔板内，每组设置3个复孔。MC3T3-E1细胞以1×10^{4}个/孔的密度接种于膜表面，待细胞贴壁24 h后，更换为成骨诱导培养基，每2 d换液1次。培养7 d后，移除培养基，PBS清洗2次，每孔加入100 μL Western及IP细胞裂解液，冰上裂解30 min。收集裂解液，于4 ℃、12 000 r/min离心15 min，取上清液。按照ALP活性检测试剂盒说明书操作，于酶标仪405 nm波长处检测各孔吸光度（OD值）。

1.3.5　茜素红染色评估矿化结节形成　MC3T3-E1细胞培养方法与各组静电纺丝膜的裁剪、灭菌及固定方法1.3.1。将膜片灭菌后铺于1个12孔板内，每组设置3个复孔。MC3T3-E1细胞以3×10^{4}个/孔的密度接种。培养1 d后更换为成骨诱导液，每2 d换液。经过21 d培养，移除原有培养液，加入4%多聚甲醛固定细胞30 min，使用0.2%茜素红染液染色30 min，用去离子水冲洗，于倒置显微镜下观察并拍照。

1.3.6　RT-qPCR检测成骨相关基因表达　MC3T3-E1细胞培养方法同1.3.1。将各组静电纺丝膜裁剪成直径为35 mm圆片，灭菌及固定方法同1.3.1。将膜片平铺于2个6孔板中，每组设置3个复孔，细胞以1×10^{5}个/孔接种。成骨诱导液培养7 d，使用TRizol试剂按照说明书步骤提取各组细胞总RNA，经超微量紫外可见分光光度计检测纯度与浓度后，取1 μg RNA逆转录为cDNA。以cDNA为模板，采用SYBR Green染料法进行qPCR扩增，目标基因包括Runx2（Runt-related transcription factor 2，Runx2）、骨保护素（osteoprotegerin，OPG），内参基因为GAPDH。引物序列如表1所示。

表1　PCR引物序列表

Table 1　PCR primer sequence table

Gene	Primer sequences
GAPDH	Forward: 5'-AAATGGTGAAGGTCGGTGTGAAC-3'
	Reverse: 5'-CAACAATCTCCACTTTGCCACTG-3'
OPG	Forward: 5'-AGGTTCCTGCACAGCTTCACAA-3'
	Reverse: 5'-AAACAGCCCAGTGACCATTCCTA-3'
Runx2	Forward: 5'-TCAGTAAGAAGAGCCAGGCAGG-3'
	Reverse: 5'-GTGTAGGTAAAGGTGGCTGGGT-3'

OPG: osteoprotegerin; Runx2: Runt-related transcription factor 2

1.3.7　Western blot检测成骨相关蛋白表达　各组静电纺丝膜处理步骤与MC3T3-E1细胞接种步骤同1.3.6，各组成骨诱导液培养7 d后制备细胞裂解液，在4 ℃、12 000 r/min条件下离心15 min，取上清液。按照BCA蛋白浓度定量试剂盒说明书操作，检测蛋白浓度。蛋白经十二烷基硫酸钠-聚丙烯酰胺凝胶电泳（SDS-PAGE）后，在30 mA条件下转膜60 min至聚偏二氟乙烯（polyvinylidene fluoride，PVDF）膜上。使用含5%脱脂奶粉的TBST（Tris-buffered saline with Tween 20，TBST）缓冲液在室温条件下封闭膜2 h，根据相对分子质量剪膜后分别与OPG抗体、Runx2抗体（1∶1 000）在4 ℃下孵育12 h。加入二抗孵育1 h，TBST再次洗膜。经ECL混合液化学发光显影，凝胶成像系统采集图像，以GAPDH为内参进行灰度分析。

1.4　统计学分析

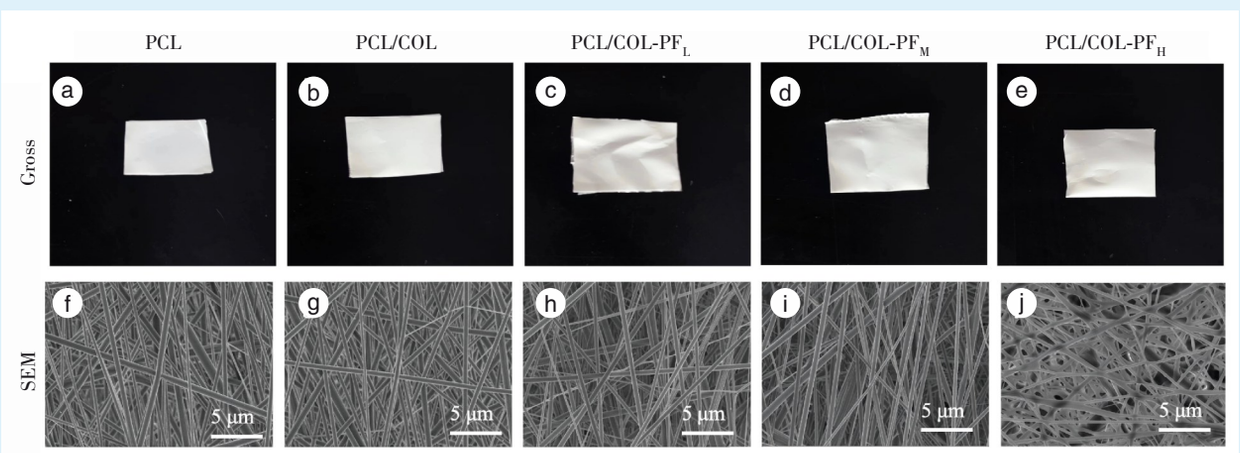
所有实验均行生物学独立重复3次，n值代表独立实验生物学重复次数。应用GraphPad Prism 9.0、Image J、Origin2021软件进行统计分析与绘图。数据首先采用Shapiro-Wilk检验进行正态性分析，符合正态分布的数据以均值±标准差（$\bar{x}\pm s$）表示。

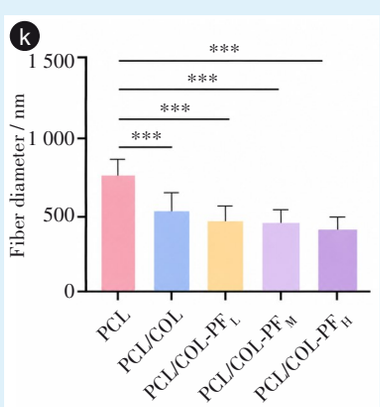
两组间比较采用独立样本t检验，多组间比较采用单因素方差分析，进一步两两比较采用Tukey多重比较检验。$P<0.05$为差异具有统计学意义。

2　结　果

2.1　静电纺丝膜的理化性能表征

2.1.1　静电纺丝膜的微观形貌与结构特征　如图1所示，5组静电纺丝膜未见明显差异，材料表面均匀光滑，无明显的颗粒和凸起。PCL组、PCL/COL组静电纺丝膜纤维均匀拉伸，纤维排列无序、分散，形成大小不一的孔隙。PCL组纤维直径为（764.0±34.3）nm，PCL/COL组为（508.8±11.1）nm，PCL/COL-PF_L为（456.6±15.8）nm，PCL/COL-PF_M为（432.0±34.1）nm，PCL/COL-PF_H为（388.5±41.4）nm，与PCL组相比，其余各组纤维直径均减少（$P<0.001$）。





a-e: representative images of the gross appearance of three biologically independent samples; the five groups showed no obvious differences, with uniformly smooth surfaces and no obvious particles or protrusions. f-j: representative SEM images from three biologically independent samples; the electrospun fibers in the PCL and PCL/COL groups were uniformly stretched and randomly distributed, forming pores of varying sizes. Upon paeoniflorin loading, the fiber diameter decreased. k: fiber diameter distribution of the electrospun membranes. The fiber diameters of the different groups were statistically analyzed using one-way analysis of variance (ANOVA), followed by Tukey's multiple comparisons test. n = 3 biologically independent samples. Compared with the PCL group, all the other groups showed significantly smaller fiber diameters (***P < 0.001). SEM: scanning electron microscopy; PCL: polycaprolactone group; PCL/COL: polycaprolactone/collagen group; PCL/COL-PF_L polycaprolactone/collagen loaded with 0.1 mg/mL of paeoniflorin group; PCL/COL-PF_M: polycaprolactone/collagen loaded with 0.2 mg/mL of paeoniflorin group; PCL/COL-PF_H: polycaprolactone/collagen loaded with 0.4 mg/mL of paeoniflorin group

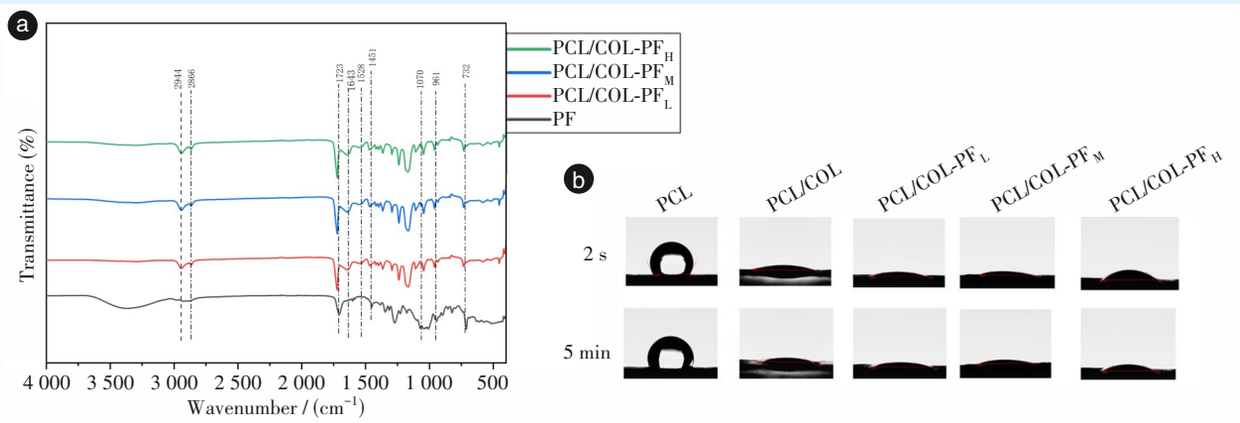
Figure 1　Macroscopic morphology and SEM microstructure of the electrospun membranes

图1　静电纺丝膜的宏观形貌和扫描电镜下微观结构

2.1.2　静电纺丝膜的化学组成及亲水性分析　傅里叶变换红外光谱检测结果（图2a）显示：2 944、2 866 cm^{-1}处是PCL的C-H的伸缩振动吸收峰，1 723 cm^{-1}处是PCL和芍药苷上的C=O的伸缩振动吸收峰，1 643 cm^{-1}处的吸收峰是COL上的（酰胺Ⅰ带）C=O的伸缩振动，1 528 cm^{-1}处的吸收峰是COL上的（酰胺Ⅱ带）N-H的弯曲振动，961和732 cm^{-1}处是芍药苷上的C-H的面外弯曲振动吸收峰。1 070 cm^{-1}处是芍药苷的苷键特征峰，在不同芍药苷含量的静电纺丝膜的红外曲线上可以看到3种物质的特征吸收峰，说明复合成功。各组静电纺丝膜特征峰相似，说明静电纺丝膜制备过程中，各组分的结构成分未发生明显变化。

静态接触角检测结果（图2b，表2）显示：与PCL组相比，PCL/COL、PCL/COL-PF_L、PCL/COL-PF_M与PCL/COL-PF_H组接触角显著减小（$P<0.001$），亲水性显著提高。

2.1.3　静电纺丝膜的体外药物释放与降解行为　体外药物释放实验结果显示（图3a、3b），每组静电纺丝膜在第1天都出现了不同程度的突释现象，PCL/



a: representative FTIR spectra of the electrospun fibrous membranes in each group from three biologically independent samples. On the infrared spectra of fiber membranes with different paeoniflorin contents, the characteristic absorption peaks of the three components were observed, indicating successful composite formation. b: representative images of the static contact angles of each group of the electrospun membranes from three biologically independent samples. The PCL group exhibited the largest static water contact angles, all exceeding 90°, indicative of its relatively poor hydrophilicity. Incorporation of COL significantly enhanced hydrophilicity, as evidenced by a marked reduction in the static water contact angle. PCL: polycaprolactone group; PCL/COL: polycaprolactone/collagen group; PCL/COL-PF$_L$: polycaprolactone/collagen loaded with 0.1 mg/mL of paeoniflorin group; PCL/COL-PF$_M$: polycaprolactone/collagen loaded with 0.2 mg/mL of paeoniflorin group; PCL/COL-PF$_H$: polycaprolactone/collagen loaded with 0.4 mg/mL of paeoniflorin group; FTIR: Fourier transform infrared spectroscopy

Figure 2　FTIR and static contact single detection results of the electrospun membranes

图2　静电纺丝膜的傅里叶变换红外光谱及静态接触角检测结果

表2　静电纺丝膜滴加超纯水后的静态接触角

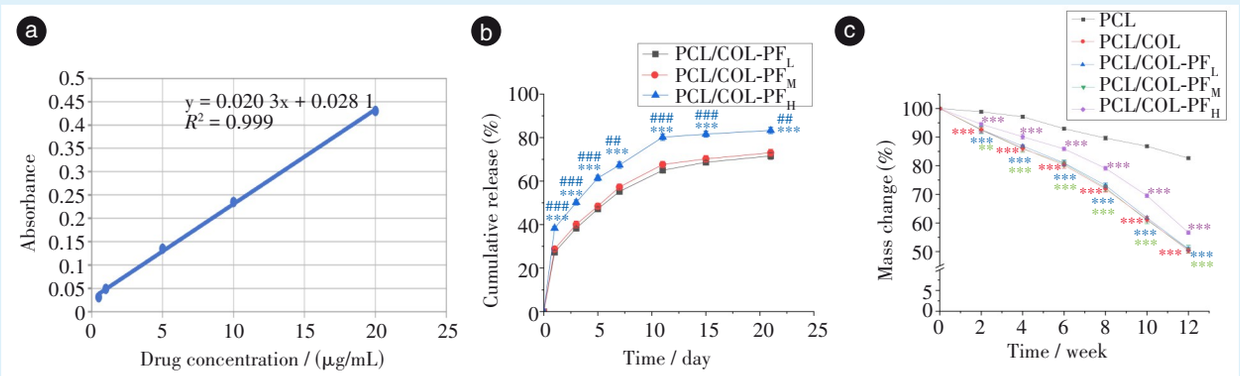
Table 2　Static water contact angles of the electrospun membranes　　$\bar{x}\pm s$, n=3

Groups	2 s(°)	5 min(°)	t	P
PCL	115.2±0.8	99.3±0.5	29.19	<0.001
PCL/COL	14.3±0.6^{a}	12.6±1.0^{a}	2.44	0.071
PCL/COL-PF$_L$	15.6±0.7^{a}	13.3±0.5^{a}	4.63	0.010
PCL/COL-PF$_M$	13.5±0.9^{ac}	12.6±0.4^{a}	1.58	0.189
PCL/COL-PF$_H$	31.5±0.8^{abcd}	25.2±0.6^{abcd}	10.91	<0.001
F	9 777.8	10 314.0		
P	<0.001	<0.001		

Statistical differences among the groups were analyzed using one-way analysis of variance (ANOVA), followed by Tukey's multiple comparisons test. a: P < 0.001 *vs.* PCL group; b: P < 0.001 *vs.* PCL/COL group; c: P < 0.001 *vs.* PCL/COL-PF$_L$ group; d: P < 0.001 *vs.* PCL/COL-PF$_M$ group. PCL: polycaprolactone group; PCL/COL: polycaprolactone/collagen group; PCL/COL-PF$_L$: polycaprolactone/collagen loaded with 0.1 mg/mL of paeoniflorin group; PCL/COL-PF$_M$: polycaprolactone/collagen loaded with 0.2 mg/mL of paeoniflorin group; PCL/COL-PF$_H$: polycaprolactone/collagen loaded with 0.4 mg/mL of paeoniflorin group

COL-PF$_L$、PCL/COL-PF$_M$及PCL/COL-PF$_H$组的释放量分别为27.2%±0.8%、28.8%±1.1%、38.3%±0.9%，7 d后药物释放速率减缓，各组静电纺丝膜均可持续释放21 d。与PCL/COL-PF$_L$、PCL/COL-PF$_M$组相比，PCL/COL-PF$_H$组药物释放较快，具有统计学差异（P<0.01）。

体外降解实验显示（图3c），PCL组第12周剩余质量比为82.67%±0.38%，累计质量损失仅约17%，降解过程缓慢且速率较为平稳；引入COL后，膜的降解速率明显加快，PCL/COL组12周剩余质量比降至56.63%±0.68%（P<0.001）；引入芍药苷后，降解速率进一步提升，PCL/COL-PF$_L$、PCL/COL-PF$_M$及PCL/COL-PF$_H$组第12周剩余质量比分别为50.94%±0.74%、50.84%±1.39%和50.33%±0.75%，3组累计质量损失均接近膜初始质量的50%，与PCL组相比均具有统计学差异（P<0.01）。



a: paeoniflorin standard curve. Paeoniflorin standard solutions (0.5, 1, 5, 10, and 20 μg/mL) were prepared, and the absorbance at 230 nm was measured to construct a paeoniflorin standard curve. b: *in vitro* drug release curve of paeoniflorin (n = 3 biologically independent samples). Statistical differences among the groups were analyzed using one-way analysis of variance (ANOVA), followed by Tukey's multiple comparisons test compared with the PCL/COL-PF$_L$ group, ***P < 0.001; compared with the PCL/COL-PF$_M$ group, ##P < 0.01; ###P < 0.001. c: degradation profiles, expressed as the residual mass ratio of scaffolds *in vitro* in each group from three biologically independent samples. Statistical differences among the groups were analyzed using one-way ANOVA, followed by Tukey's multiple comparisons test, compared with the PCL group, **P < 0.01,***P < 0.001. Data were presented as the mean ± SD. PCL: polycaprolactone group; PCL/COL: polycaprolactone/collagen group; PCL/COL-PF$_L$: polycaprolactone/collagen loaded with 0.1 mg/mL of paeoniflorin group; PCL/COL-PF$_M$: polycaprolactone/collagen loaded with 0.2 mg/mL of paeoniflorin group; PCL/COL-PF$_H$: polycaprolactone/collagen loaded with 0.4 mg/mL of paeoniflorin group

Figure 3　Results of *in vitro* drug release and *in vitro* degradation of electrospun membranes

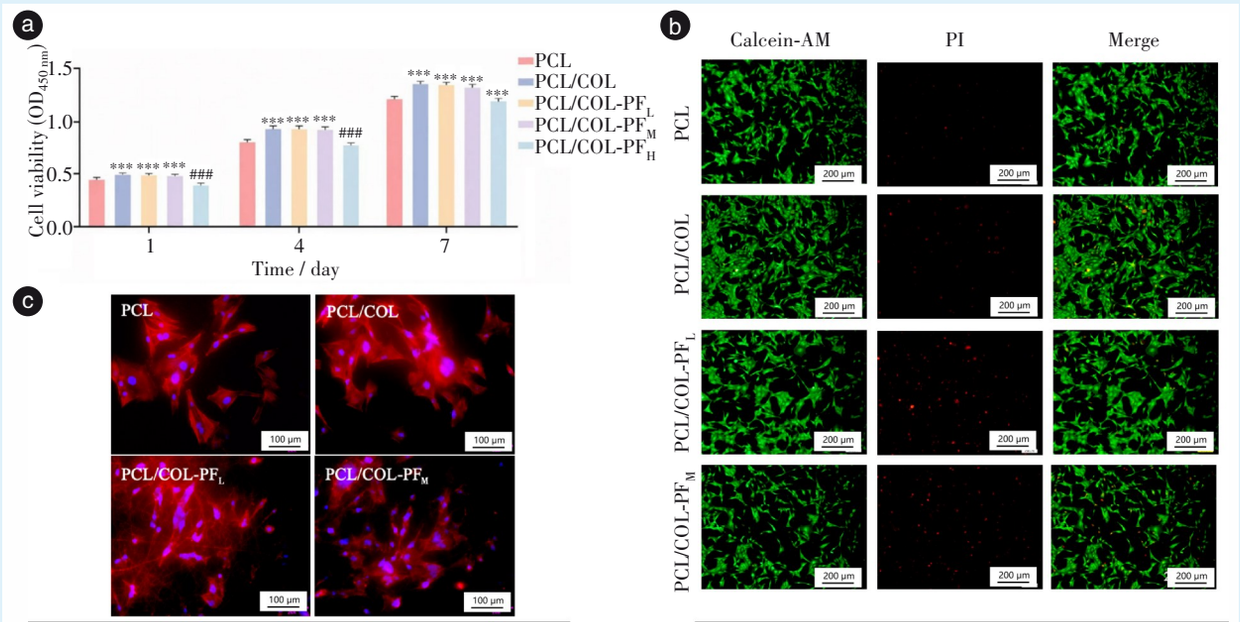
图3　静电纺丝膜的体外药物释放情况及体外降解情况结果

2.2　负载芍药苷的复合支架对MC3T3-E1细胞生物学行为的影响

2.2.1　细胞相容性评价　CCK8检测显示(图4a)，第1、4、7天PCL/COL组、PCL/COL-PF$_L$组及PCL/COL-PF$_M$对比PCL组表现出促进细胞增殖的效果(P<0.001)；而PCL/COL-PF$_H$组第1、4天与PCL组比较差异无统计学意义(P>0.05)，第7天则显著抑制细胞增殖(P<0.001)。活/死细胞染色结果如图4b所示，不同组间膜上细胞的数量没有明显区别，以绿色荧光为主，红色荧光极少。罗丹明-鬼笔环肽染色如图4c示，所有电纺纤维膜表面均有细胞黏附和生长，且细胞状态良好。PCL/COL-PF$_L$、PCL/COL-PF$_M$组静电纺丝膜结构清晰，表明各组静电纺丝膜对MC3T3-E1细胞无明显毒性，生物相容性良好。结合CCK-8检测结果，后续成骨分化实验选取PCL、PCL/COL、PCL/COL-PF$_L$及PCL/COL-PF$_M$ 4组进行。

2.2.2　对细胞早期成骨分化及矿化的影响　ALP染色如图5a所示，各组均呈阳性反应且着色均匀，与PCL组、PCL/COL组相比，PCL/COL-PF$_L$组与PCL/COL-PF$_M$组染色加深，且随着药物负载量的增加，染色面积和染色程度均随之增加。ALP活性结果图5b所示，细胞接种后的第7天，与PCL组比较，PCL/COL-PF$_L$组及PCL/COL-PF$_M$组ALP活性有显著增强(P<0.001)；PCL/COL-PF$_M$组最为明显。茜素红染色结果(图5a)表明，各组静电纺丝膜均可见到明显的矿化。PCL组矿化结节较少，染色面积最小；PCL/COL组矿化结节增多，染色面积增大；PCL/COL-PF$_L$和PCL/COL-PF$_M$组染色面积进一步增大，而且染色面积大小随载药浓度升高而增大。

2.2.3　成骨相关基因及蛋白表达水平的检测　RT-qPCR检测结果(图6a、6b)显示，与PCL组相比，PCL/COL组Runx2 mRNA表达显著升高(P<0.05)，OPG mRNA表达呈升高趋势但差异无统计学意义(P>0.05)。PCL/COL-PF$_L$组和PCL/COL-PF$_M$组的Runx2和OPG mRNA表达水平均高于PCL组(P<0.01)；其中PCL/COL-PF$_M$组表达水平最高，显著高于PCL组和PCL/COL组(P<0.001)。Western blot检测结果(图6c~6e)显示，各蛋白表达趋势与基因检测结果基本一致：与PCL组相比，PCL/COL组Runx2蛋白表达水平升高(P<0.05)，OPG蛋白表达水平升高但差异无统计学意义(P>0.05)；PCL/COL-PF$_L$组和PCL/COL-PF$_M$组的Runx2和OPG蛋白表达水平均显著高于PCL组(P<0.001)，且PCL/COL-PF$_M$组表达水平最明显。



a: proliferation results of scaffold cells in each group (n = 3 biologically independent replicates). Data for proliferation were analyzed by one-way ANOVA followed by Tukey's post-hoc test. Data were presented as the mean ± SD. Compared with the PCL group, *** P < 0.001; compared with the PCL/COL group, ###P < 0.001. b: representative images of live/dead staining from three biologically independent replicates of MC3T3-E1 cells cultured on the electrospun scaffolds. Green fluorescence (Calcein-AM) indicated live cells, while red fluorescence (PI) indicated dead cells. No obvious differences in cell numbers were observed among the groups, with green fluorescence predominating and minimal red fluorescence detected across all scaffolds. c: representative cytoskeletal staining images from three biologically independent replicates of MC3T3-E1 cells cultured on the electrospun membranes in each group. Cell adhesion and spreading were observed on the surfaces of all membranes, with clear cytoskeletal morphology and good cell morphology. PCL: MC3T3-E1 cells were cultured on polycaprolactone membranes pre-immersed in α-MEM medium. PCL/COL: MC3T3-E1 cells were cultured on polycaprolactone/collagen membranes pre-immersed in α-MEM medium; PCL/COL-PF_L: MC3T3-E1 cells were cultured on polycaprolactone/collagen membranes loaded with 0.1 mg/mL of paeoniflorin, pre-immersed in α-MEM medium; PCL/COL-PF_M: MC3T3-E1 cells were cultured on polycaprolactone/collagen membranes loaded with 0.2 mg/mL of paeoniflorin, pre-immersed in α-MEM medium; PCL/COL-PF_H: MC3T3-E1 cells were cultured on polycaprolactone/collagen membranes loaded with 0.4 mg/mL of paeoniflorin, pre-immersed in α-MEM medium. Calcein-AM: Calcein acetoxymethyl ester; PI: propidium iodide

Figure 4　Biocompatibility results of the electrospun scaffolds in each group

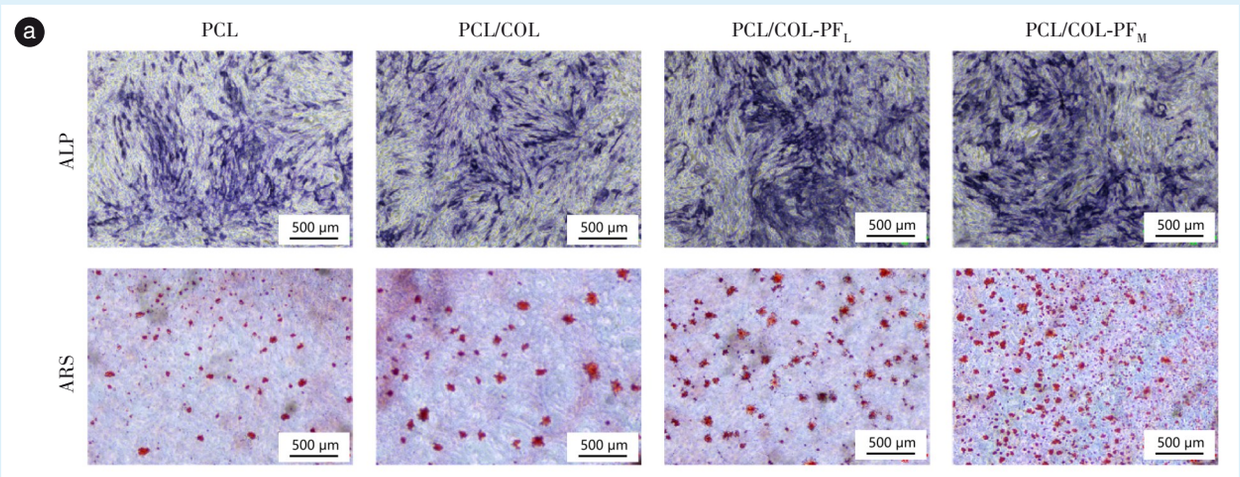
图4　各组静电纺丝膜的生物相容性结果

3　讨　论

骨组织工程支架的核心挑战在于同时满足结构支撑、细胞相容性和生物活性三重功能[16-17]。本研究基于这一需求，构建了负载芍药苷的PCL/COL静电纺丝膜，并系统评估了其理化性能、生物相容性及促成骨效应。

已有研究表明，淫羊藿苷、槲皮素等天然活性单体负载于静电纺丝膜后均可促进成骨细胞增殖与分化[18-19]。与上述药物类似，芍药苷同样具有促进成骨分化及调节骨代谢的作用。芍药苷是传统中药白芍的主要活性成分，研究表明芍药苷不仅能够抑制NF-κB信号通路来降低破骨细胞的分化功能、缓解类风湿关节炎患者骨丢失的症状[20]，也可以通过Wnt/β-catenin信号通路促进成骨分化，上调相关成骨基因ALP、骨钙素（osteocalcin，OCN）、骨桥蛋白（osteopontin，OPN）和Runx2的表达[21-23]。

静电纺丝技术可制备高比表面积、高孔隙率的纳米纤维支架，模拟天然骨细胞外基质的微观结构[24-25]。本研究中，COL的引入显著改善了PCL支架的亲水性和降解速率，这与COL富含极性基团及酶解位点的特性一致[26]。在骨组织工程领域，构建纳米纤维支架的核心策略在于调控三维支架材料与宿主细胞间的动态交互作用，COL作为受体介导信号的调节因子，可以精确控制细胞行为[27-28]。Ⅰ型COL的三维网状结构能够模拟ECM的天然环境[29-30]。当细胞与胶原支架接触时，其表面的整合素受体能够识别COL中的精氨



a: representative ALP and ARS staining images from three biologically independent replicates of MC3T3-E1 cells cultured on the four scaffolds. The scaffolds in the PCL/COL-PF$_M$ group exhibited the deepest staining and the highest number of calcified nodules. b: as shown by the ALP activity results, compared with the PCL group, ALP activity was significantly enhanced in the PCL/COL-PF$_L$ and PCL/COL-PF$_M$ groups ($P < 0.001$), with the most pronounced enhancement observed in the PCL/COL-PF$_M$ group ($n = 3$ biologically independent replicates). Data were analyzed by one-way ANOVA followed by Tukey's post-hoc test. Data were presented as the mean ± SD. Compared with the PCL group, ***$P < 0.001$. PCL: MC3T3-E1 cells were cultured on polycaprolactone membranes pre-immersed in α-MEM medium. PCL/COL: MC3T3-E1 cells were cultured on polycaprolactone/collagen membranes pre-immersed in α-MEM medium; PCL/COL-PF$_L$: MC3T3-E1 cells were cultured on polycaprolactone/collagen membranes loaded with 0.1 mg/mL of paeoniflorin, pre-immersed in α-MEM medium; PCL/COL-PF$_M$: MC3T3-E1 cells were cultured on polycaprolactone/collagen membranes loaded with 0.2 mg/mL of paeoniflorin, pre-immersed in α-MEM medium. All staining experiments were independently repeated three times with similar results. ALP: alkaline phosphatase ARS: Alizarin Red S staining

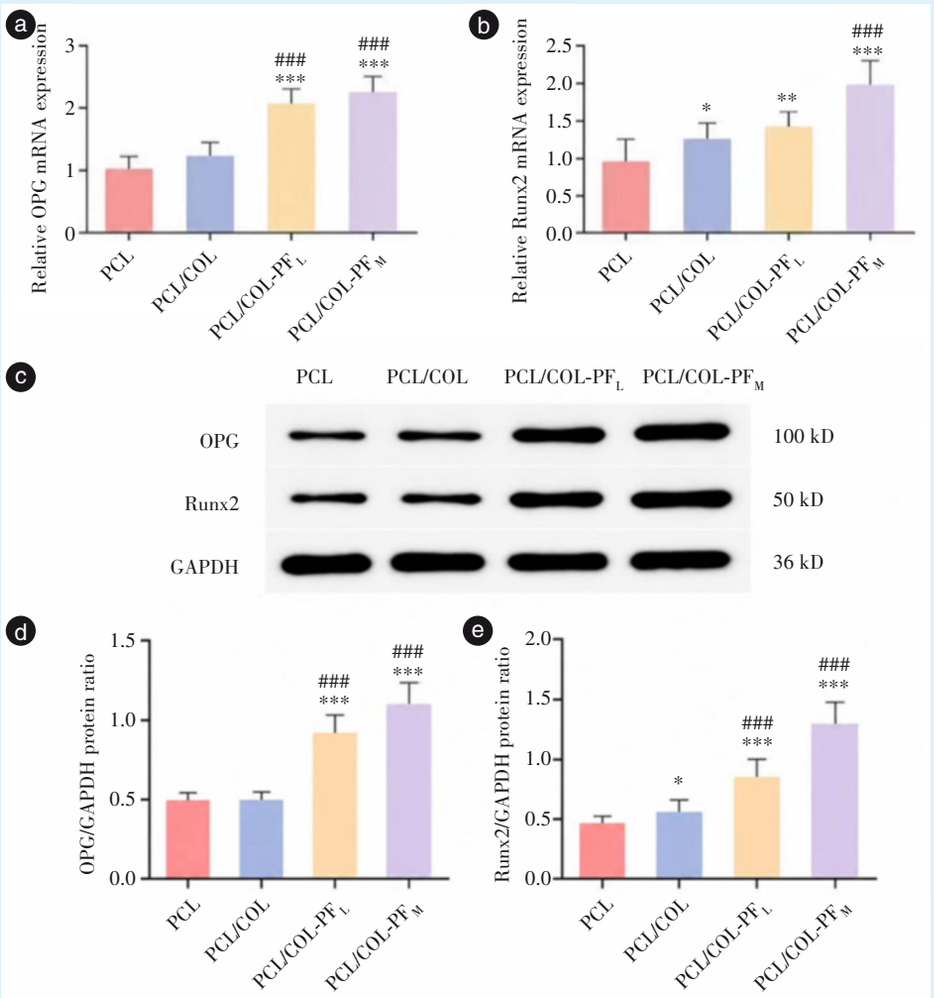
Figure 5　Effects of the electrospun membranes from each group on the osteogenic differentiation of MC3T3-E1 cells

图5　各组静电纺丝膜对MC3T3-E1细胞成骨分化的影响

酸-甘氨酸-天冬氨酸序列，从而激活细胞内信号通路，影响细胞的增殖，提升细胞的存活率[31-32]。PCL作为一种人工合成的高分子材料，具有良好的力学性能与溶解性，但生物活性相对较弱[33]。

SEM观察显示，各组纤维呈无规则网状结构，孔隙分布均匀。芍药苷的加入使纤维直径减小，推测与芍药苷分子中多个羟基提高溶液导电性、增强射流拉伸细化有关[4]。FTIR结果证实各组分特征峰均被检出，载药制备未改变各组分的化学结构。静态接触角结果显示，COL的加入显著提升了材料亲水性，而芍药苷对亲水性无明显影响，提示COL是改善PCL/COL复合膜亲水性的主要因素。共混电纺可使支架实现局部药物缓释[34]。本研究中3组载药膜在第1天均出现不同程度突释，该现象在低分子量药物封装于电纺纤维中时较为常见[35]；此后进入缓慢释放阶段，21 d内累积释放率达70%～80%，表明支架具有良好的缓释性能。体外降解实验表明，COL的引入显著加快了PCL的降解速率，芍药苷的进一步加入使降解速率进一步提升。COL与芍药苷对降解的促进作用可能与共混载药增加纤维孔隙率有关[36]，但本研究未对孔隙率进行定量测定，其具体机制有待后续验证。上述结果表明，载药浓度的变化未明显影响支架的纤维形貌及亲水性，这为本研究进一步系统比较不同载药浓度、筛选最优浓度提供了材料学基础。

CCK-8结果显示，PCL/COL-PF$_H$组在第7天表现出细胞增殖抑制，可能与纤维直径过小（388 nm）导致孔隙率下降、不利于细胞三维伸展有关。结合活/死细胞染色结果（各组活细胞占绝大多数）推



a-b: relative OPG and Runx 2 mRNA expression in each group (n = 3 biologically independent replicates). c: representative western blot images of Runx2, OPG, and GAPDH protein expression in MC3T3-E1 cells cultured on the four electrospun membranes. d-e: densitometric quantification of Runx2 and OPG protein expression normalized to GAPDH (n = 3 biologically independent replicates). Statistical comparisons were performed using one-way ANOVA followed by Tukey's post hoc test. Data were presented as the mean ± SD. Compared with the PCL group, *P < 0.05; **P < 0.01; ***P < 0.001; compared with the PCL/COL group, ###P < 0.001. PCL: MC3T3-E1 cells were cultured on polycaprolactone membranes pre-immersed in α -MEM medium. PCL/COL: MC3T3-E1 cells were cultured on polycaprolactone/collagen membranes pre-immersed in α -MEM medium. PCL/COL-PF$_L$: MC3T3-E1 cells were cultured on polycaprolactone/collagen membranes loaded with 0.1 mg/mL of paeoniflorin, pre-immersed in α-MEM medium. PCL/COL-PF$_M$: MC3T3-E1 cells were cultured on polycaprolactone/collagen membranes loaded with 0.2 mg/mL of paeoniflorin, pre-immersed in α-MEM medium. OPG: osteoprotegerin; Runx2: Runt-related transcription factor 2

Figure 6　Effects of the electrospun membranes in each group on the expression of osteogenesis-related genes and proteins in MC3T3-E1 cells

图 6　各组静电纺丝膜对MC3T3-E1细胞成骨相关基因及蛋白表达的影响

测，该抑制效应并非急性细胞毒性所致，其具体机制有待进一步研究。罗丹明-鬼笔环肽染色显示各组细胞黏附铺展良好，表明COL的引入显著增强了细胞-材料相互作用[37]。

成骨相关实验结果显示，PCL/COL-PF$_M$组的ALP活性和矿化结节形成最为显著。RT-qPCR和Western blot结果进一步表明，COL的加入可上调Runx2表达，负载芍药苷后Runx2和OPG的表达水平进一步提高。OPG通过维持RANKL/RANK/OPG平衡抑制破骨细胞分化，为成骨创造有利环境[38-39]；Runx2是调控成骨分化的核心转录因子[40-41]。上述结果提示，COL与芍药苷在促成骨方面具有协同效应——COL提供利于细胞黏附的微环境，芍药苷则通过经典信号通路上调成骨相关基因表达，二者共同促进了MC3T3-E1细胞的成骨分化。

本研究的创新之处主要体现在以下三点：①比较了三种载药浓度（0.1、0.2、0.4 mg/mL）芍药苷负载PCL/COL静电纺丝膜的理化性能和成骨活性，明确了0.2 mg/mL为最优载药浓度；②揭示了COL与芍药苷在上调Runx2和OPG表达方面的协同增效作用；③将纤维形貌、亲水性、降解行为、药物释放、生物相容性与成骨活性纳入同一体系进行比较，结果更具整体性和可比性。

本研究仍存在一定局限性：①未与淫羊藿苷、槲皮素等天然药物进行横向对照；②复合支架的系统力学表征及体内动物实验有待补充；③细胞黏附率及细胞迁移行为尚缺乏定量数据。后续研究将在统一支架体系下引入上述实验，以期对该支架的促成骨机制及综合性能作出更为系统的评价。

【Author contributions】 Li ZH carried out the experiments and wrote the manuscript. Liu ZH and Yang YZ analyzed the data, and revised the manuscript. Zhang B and Zhang YT conceived the study and reviewed the manuscript. All authors read and approved the final version of the manuscript before submission.

【Ethics statement】 The authors have nothing to report.

【Funding】 This study was supported by the Natural Science Foundation of Shandong Province (No. ZR2023MH039), the Research Project of the Affiliated Hospital of Binzhou Medical University (No. BY2021KJ10), and the National Innovation and Entrepreneurship Training Program for College Students (No. 202310440160). The funder had no role in the study design, data collection and analysis, decision to publish, or preparation of the manuscript.

【Competing interests】 All authors have completed the ICMJE uniform disclosure form at www.icmje.org/disclosure-of-interest/ and declare: support from the Natural Science Foundation of Shandong Province (No. ZR2023MH039), the Research Project of the Affiliated Hospital of Binzhou Medical University (No. BY2021KJ10), and the National Innovation and Entrepreneurship Training Program for College Students (No. 202310440160) for the submitted work; no financial relationships with any organisations that might have an interest in the submitted work in the previous three years; no other relationships or activities that could appear to have influenced the submitted work.

【Data availability statement】 The original contributions presented in this study are included in the article. Further inquiries can be directed to the corresponding author upon reasonable request.

【Generative AI statement】 The authors declared that generative AI was not used in the creation of this manuscript.

参考文献

[1] Wang J, Liu M, Yang C, et al. Biomaterials for bone defect repair: types, mechanisms and effects[J]. Int J Artif Organs, 2024, 47(2): 75-84. doi: 10.1177/03913988231218884.

[2] López JM. Bone development and growth[J]. Int J Mol Sci, 2024, 25(12): 6767. doi: 10.3390/ijms25126767.

[3] Fan L, Ren Y, Emmert S, et al. The use of collagen-based materials in bone tissue engineering[J]. Int J Mol Sci, 2023, 24(4): 3744. doi: 10.3390/ijms24043744.

[4] Chinnappan BA, Krishnaswamy M, Xu H, et al. Electrospinning of biomedical nanofibers/nanomembranes: effects of process parameters[J]. Polymers, 2022, 14(18): 3719. doi: 10.3390/polym14183719.

[5] Maliszewska I, Czapka T. Electrospun polymer nanofibers with antimicrobial activity[J]. Polymers, 2022, 14(9): 1661. doi: 10.3390/polym14091661.

[6] Yan B, Zhang Y, Li Z, et al. Electrospun nanofibrous membrane for biomedical application[J]. SN Appl Sci, 2022, 4(6): 172. doi: 10.1007/s42452-022-05056-2.

[7] Raja IS, Preeth DR, Vedhanayagam M, et al. Polyphenols-loaded electrospun nanofibers in bone tissue engineering and regeneration [J]. Biomater Res, 2021, 25(1): 29. doi: 10.1186/s40824-021-00229-3.

[8] Siddiqui N, Asawa S, Birru B, et al. PCL-based composite scaffold matrices for tissue engineering applications[J]. Mol Biotechnol, 2018, 60(7): 506-532. doi: 10.1007/s12033-018-0084-5.

[9] Gharibshahian M, Salehi M, Beheshtizadeh N, et al. Recent advances on 3D-printed PCL-based composite scaffolds for bone tissue engineering[J]. Front Bioeng Biotechnol, 2023, 11: 1168504. doi: 10.3389/fbioe.2023.1168504.

[10] Zheng M, Wang X, Chen Y, et al. A review of recent progress on collagen-based biomaterials[J]. Adv Healthc Mater, 2023, 12(16): e2202042. doi: 10.1002/adhm.202202042.

[11] Sousa AC, Alvites R, Lopes B, et al. Hybrid scaffolds for bone tissue engineering: integration of composites and bioactive hydrogels loaded with hDPSCs[J]. Biomater Adv, 2025, 166: 214042. doi: 10.1016/j.bioadv.2024.214042.

[12] Ni J, Yang D, Song L, et al. Protective effects of paeoniflorin on alveolar bone resorption and soft-tissue breakdown in experimental periodontitis[J]. J Periodontal Res, 2016, 51(2): 257-264. doi: 10.1111/jre.12305.

[13] Shi G, Yang C, Wang Q, et al. Traditional Chinese medicine compound-loaded materials in bone regeneration[J]. Front Bioeng Biotechnol, 2022, 10: 851561. doi: 10.3389/fbioe.2022.851561.

[14] He T, Wang J, Huang P, et al. Electrospinning polyvinylidene fluoride fibrous membranes containing anti-bacterial drugs used as wound dressing[J]. Colloids Surf B Biointerfaces, 2015, 130: 278-286. doi: 10.1016/j.colsurfb.2015.04.026.

[15] Promnil S, Ruksakulpiwat C, Numpaisal PO, et al. Electrospun poly(lactic acid) and silk fibroin based nanofibrous scaffold for meniscus tissue engineering[J]. Polymers, 2022, 14(12): 2435. doi: 10.3390/polym14122435.

[16] Percival KM, Paul V, Husseini GA. Recent advancements in bone tissue engineering: integrating smart scaffold technologies and bioresponsive systems for enhanced regeneration[J]. Int J Mol Sci, 2024, 25(11): 6012. doi: 10.3390/ijms25116012.

[17] Schulze F, Lang A, Schoon J, et al. Scaffold guided bone regeneration for the treatment of large segmental defects in long bones[J]. Biomedicines, 2023, 11(2): 325. doi: 10.3390/biomedicines11020325.

[18] Zhang M, Huang Z, Wang X, et al. Personalized PLGA/BCL scaffold with hierarchical porous structure resembling periosteum-bone complex enables efficient repair of bone defect[J]. Adv Sci, 2024, 11(35): 2401589. doi: 10.1002/advs.202401589.

[19] Hu Y, Fu Z, Yang S, et al. A multifunctional quercetin/polycaprolactone electrospun fibrous membrane for periodontal bone regeneration[J]. Mater Today Bio, 2023, 24: 100906. doi: 10.1016/j.mtbio.2023.100906.

[20] Xu H, Cai L, Zhang L, et al. Paeoniflorin ameliorates collagen-induced arthritis *via* suppressing nuclear factor-κB signalling pathway in osteoclast differentiation[J]. Immunology, 2018, 154(4): 593-603. doi: 10.1111/imm.12907.

[21] Guo W, Yang XG, Shi YL, et al. The effects and mechanism of paeoniflorin in promoting osteogenic differentiation of MC3T3-E1 [J]. J Orthop Surg Res, 2022, 17(1): 90. doi: 10.1186/s13018-022-02965-1.

[22] Wang Y, Dai J, Zhu Y, et al. Paeoniflorin regulates osteoclastogenesis and osteoblastogenesis *via* manipulating NF- κB signaling pathway both *in vitro* and *in vivo*[J]. Oncotarget, 2017, 9(7): 7372-7388. doi: 10.18632/oncotarget.23677.

[23] 杨立宇, 郭然, 牟帅, 等. 芍药苷促进小鼠成骨分化抗骨质疏松作用的实验研究[J]. 中国骨质疏松杂志, 2020, 26(12): 1742-1748, 1759. doi: 10.3969/j.issn.1006-7108.2020.12.005.
Yang LY, Guo R, Mu S, et al. Experimental study on the effect of paeoniflorin in promoting osteogenic differentiation and anti-osteoporosis in mice[J]. Chin J Osteoporos, 2020, 26(12): 1742-1748, 1759. doi: 10.3969/j.issn.1006-7108.2020.12.005.

[24] Zhou Z, Cui J, Wu S, et al. Silk fibroin-based biomaterials for cartilage/osteochondral repair[J]. Theranostics, 2022, 12(11): 5103-5124. doi: 10.7150/thno.74548.

[25] Aminatun, Hanum SF, Izak RD, et al. Fabrication and compatibility evaluation of polycaprolactone/hydroxyapatite/collagen-based fiber scaffold for anterior cruciate ligament injury[J]. RSC Adv, 2023, 13(16): 10459-10467. doi: 10.1039/d2ra07756f.

[26] Gharati G, Shirian S, Sharifi S, et al. Comparison capacity of collagen hydrogel and collagen/strontium bioglass nanocomposite scaffolds with and without mesenchymal stem cells in regeneration of critical sized bone defect in a rabbit animal model[J]. Biol Trace Elem Res, 2022, 200(7): 3176-3186. doi: 10.1007/s12011-021-02909-6.

[27] Wen RM, Wang HX, Liu ZJ, et al. Nanofiber scaffold for bone tissue engineering: mechanism, challenge and future prospect[J]. World J Orthop, 2025, 16(12): 112998. doi: 10.5312/wjo. v16. i12.112998.

[28] Zhou T, C Cavalcante R, Ge C, et al. Synthetic helical peptides on nanofibers to activate cell-surface receptors and synergistically enhance critical-sized bone defect regeneration[J]. Bioact Mater, 2024, 43: 98-113. doi: 10.1016/j.bioactmat.2024.08.017.

[29] Rider P, Kačarević ŽP, Elad A, et al. Analysis of a pure magnesium membrane degradation process and its functionality when used in a guided bone regeneration model in beagle dogs[J]. Materials, 2022, 15(9): 3106. doi: 10.3390/ma15093106.

[30] Briquez PS, Tsai HM, Watkins EA, et al. Engineered bridge protein with dual affinity for bone morphogenetic protein-2 and collagen enhances bone regeneration for spinal fusion[J]. Sci Adv, 2021, 7(24): eabh4302. doi: 10.1126/sciadv.abh4302.

[31] Matinong AME, Chisti Y, Pickering KL, et al. Collagen extraction from animal skin[J]. Biology, 2022, 11(6): 905. doi: 10.3390/biology11060905.

[32] Qin D, Wang N, You XG, et al. Collagen-based biocomposites inspired by bone hierarchical structures for advanced bone regeneration: ongoing research and perspectives[J]. Biomater Sci, 2022, 10 (2): 318-353. doi: 10.1039/d1bm01294k.

[33] He X, Wang L, Lv K, et al. Polyethylene oxide assisted fish collagen-poly-ε-caprolactone nanofiber membranes by electrospinning[J]. Nanomaterials, 2022, 12(6): 900. doi: 10.3390/nano12060900.

[34] Yang Y, Zhang R, Liang Z, et al. Application of electrospun drug-loaded nanofibers in cancer therapy[J]. Polymers, 2024, 16(4): 504. doi: 10.3390/polym16040504.

[35] Cheng H, Yang X, Che X, et al. Biomedical application and controlled drug release of electrospun fibrous materials[J]. Mater Sci Eng C Mater Biol Appl, 2018, 90: 750-763. doi: 10.1016/j.msec.2018.05.007.

[36] Luo W, Wang Y, Han Q, et al. Advanced strategies for constructing interfacial tissues of bone and tendon/ligament[J]. J Tissue Eng, 2022, 13: 20417314221144714. doi: 10.1177/20417314221144714.

[37] Huo P, Han X, Zhang W, et al. Electrospun nanofibers of polycaprolactone/collagen as a sustained-release drug delivery system for artemisinin[J]. Pharmaceutics, 2021, 13(8): 1228. doi: 10.3390/pharmaceutics13081228.

[38] Gao YM, Pei Y, Zhao FF, et al. Osteoclasts in osteosarcoma: mechanisms, interactions, and therapeutic prospects[J]. Cancer Manag Res, 2023, 15: 1323-1337. doi: 10.2147/CMAR.S431213.

[39] Yin L, Sun C, Zhang J, et al. Critical signaling pathways in osteoclast differentiation and bone resorption: mechanisms and therapeutic implications for periprosthetic osteolysis[J]. Front Cell Dev Biol, 2025, 13: 1639430. doi: 10.3389/fcell.2025.1639430.

[40] Xu HJ, Liu XZ, Yang L, et al. Runx2 overexpression promotes bone repair of osteonecrosis of the femoral head (ONFH)[J]. Mol Biol Rep, 2023, 50(6): 4769-4779. doi: 10.1007/s11033-023-08411-7.

[41] Liu DD, Zhang CY, Liu Y, et al. RUNX2 regulates osteoblast differentiation *via* the BMP4 signaling pathway[J]. J Dent Res, 2022, 101(10): 1227-1237. doi: 10.1177/00220345221093518.

（编辑　罗燕鸿）

Open Access
This article is licensed under a Creative Commons Attribution 4.0 International License.
Copyright © 2026 by Editorial Department of Journal of Prevention and Treatment for Stomatological Diseases

官网